JOURNAL OF COMPUTATIONAL PHYSICS 101, 80–93 (1992)

A Relaxation Algorithm for Classical Paths as a Function of End Points: Application to the Semiclassical Propagator for Far-from-Caustic and Near-Caustic Conditions

A. G. BASILE

Laboratory of Atomic and Solid State Physics, Cornell University, Ithaca, New York 14853-2501

AND

C. G. GRAY

Guelph-Waterloo Program for Graduate Work in Physics, University of Guelph, Guelph, Ontario, Canada N1G 2W1

Received June 8, 1990; revised May 8, 1991

We present a relaxation algorithm for obtaining the classical and nonclassical paths from the boundary value problem with fixed initial and final positions and times on the path, and we discuss a technique for obtaining all paths connecting a given set of end points. From these paths, the action and other essential quantities entering the far-from-caustic and near-caustic expressions for the semiclassical propagator can be obtained. We illustrate with three one-dimensional examples —a time-dependent harmonic oscillator, a double-well anharmonic oscillator, and the repulsive $1/x^2$ potential—and find good agreement between the numerically calculated and exact paths where analytical results are available for comparison. We also find surprisingly good agreement between the semi-classical propagator and the exact propagator in cases where the latter is available for comparison.

1. INTRODUCTION

The Feynman path integral representation of the propagator is useful for a quantum mechanical formulation of many problems in equilibrium and nonequilibrium statistical mechanics [1–3]. For equilibrium problems [4], the density matrix is the propagator evaluated at purely imaginary times, and numerically the problem is viable because the discretized path integral involves integrations over a positive integrand. For nonequilibrium problems, however, involving time correlation functions of the type $\langle A(0)\, B(t)\rangle$, the propagator is required at real and complex times [5], and the integrand in the discretized path integral contains a strongly oscillatory piece. Numerically, a brute force calculation leads to massive phase cancellations and is not viable. Unfortunately, to date, this problem has not yet been solved in a satisfactory manner for all cases, although recently some promising stationary phase Monte Carlo methods have been proposed [6–8] and tested on some special cases.

An approximate approach which avoids the phase cancellation problem is the semiclassical or WKB approximation [2, 9]. There are many physical systems where quantum effects are small and a WKB approximation for the propagator is justified. Since in WKB the integration over the rapidly oscillating integrand is done analytically by a stationary phase approximation, numerically the massive phase cancellations do not arise. There has been much analytic work in the theory of WKB propagators [2, 9], but apart from Ref. [10], which deals with semiclassical path integrals in the coherent state representation, and Ref. [11], which we discuss below, little work has been done in devising discretized algorithms for calculating the quantities that enter the expression for the WKB propagator. This is true of the usual far-from-caustic expression as well as of the near-caustic expression. A caustic is a surface in path-parameter space (i.e., the space of end point variables x_0, t_0, x_n, t_n—see next paragraph) which separates the space into regions where there are typically two allowed classical paths connecting the end points on the classically allowed side of the caustic and two nonclassical paths on the other side. On the caustic itself, there is typically just one allowed classical path corresponding to each set of end point variables.

The key quantity required for the WKB propagator is the classical action as a function of end point variables on a path, (x_0, t_0) and (x_n, t_n), i.e.,

$$S_C(x_0, t_0; x_n, t_n) = \int_{(x_0, t_0)}^{(x_n, t_n)} L(x_C(t))\, dt, \qquad (1)$$

0021-9991/92 $5.00

where $x_C(t)$ is the classical path expressed as a function of end points as well as time t,

$$x_C(t) = x_C(t; x_0, t_0, x_n, t_n), \tag{2}$$

and L is the Lagrangian which is a function of the path. We assume it to have the form,

$$L(x(t)) = \tfrac{1}{2}m\dot{x}^2 - V(x, t), \tag{3}$$

where $\dot{x} = dx/dt$ and m is the mass of the particle, which moves in a time and space dependent potential [12], $V(x, t)$. In general, however, S_C is a nontrivial quantity to calculate, even numerically. The problem lies in obtaining the path *as a function of end points*, as in (2). One obvious method is to obtain the classical path by integrating the Euler–Lagrange equation, or equivalently Newton's equation, as an initial value problem and obtain, for instance,

$$x_C(t) = x_C(t; x_0, v_0, t_0), \tag{4}$$

where v_0 is the initial velocity on the path. Then, by adjusting v_0, the classical path can be made to pass through the end points, (x_0, t_0) and (x_n, t_n). This *shooting* method requires a substantial amount of work and can become numerically horrible in situations where the path is very sensitive to changes in v_0, as one can imagine for various potentials. The problem is further compounded in higher dimensions, where many parameters in (4) will need adjustment, or in obtaining paths in the classically unallowed region where v_0 will have to be made complex. One would like to avoid these numerical problems, especially in practical applications [5], where the propagator is to be integrated with respect to its end points. Then many paths will have to be generated in this manner.

The main purpose of this paper is to introduce a numerically more viable method for obtaining (2), and the other quantities such as S_C, required in the WKB expressions for the propagator, for both far-from-caustic and near-caustic conditions. Our method is based on obtaining the classical path from a *boundary value problem*, rather than from an initial value one; the problem is to find the path (or paths), given the two end points and the time taken to reach the final point. This is done by a relaxation method, similar to relaxation methods for calculating electrostatic potentials, or to Lanczos methods for the ground state in quantum problems [13].

The boundary value problem outlined in the above paragraph has been considered by Doll *et al.* [11], by a completely different method. In their method they consider the decomposition of a path into its Fourier modes and proceed to obtain the Fourier coefficients of the path by simulated annealing, a stochastic Monte Carlo process. However, by retaining our paths in real space representation, the discretized action functional in matrix language can effectively be written in tridiagonal form (consider $\delta^2\tilde{S}_{jk}$ in Section 3) and rapidly extremized by a deterministic procedure, which is not possible for the Fourier representation, where the corresponding matrix is, in general, not tridiagonal. Our formulation of the discretized action functional in real space, which leads to the tridiagonal form, is optimal for obtaining the paths, since (1) reducing the discretized action functional to diagonal form is only possible if the problem is already solved, (2) although 5, 7, ...-diagonal matrices could also be formed in real space representation (the nondiagonal piece arises from the kinetic energy term), the tridiagonal form is the simplest which can be implemented. A representation in an other basis (e.g., in Fourier modes) will not generate a tridiagonal form in general. Besides greater speed, our method also has the advantage of systematically finding *all* allowed paths connecting the two end points in a given time. Further, Doll *et al.* [11] do not discuss the following topics, which are discussed in this paper: near-caustic conditions, nonclassical paths, and the Van Vleck prefactor for the semiclassical propagator.

We organize the paper as follows. In Section 2 we introduce the discretized propagator for Lagrangians of the form (3), obtain the discretized WKB expressions for the far-from-caustic and near-caustic conditions, and we identify the essential ingredients which are needed in these, i.e., the paths, actions, and Van Vleck prefactors. In Section 3 we formally present our method for obtaining numerically those quantities needed in Section 2; in particular, we show how to determine *all* the paths connecting two end points in a given time. In Section 4 we implement our method for three examples: (a) a time-dependent harmonic potential, (b) a time-independent double-well anharmonic potential, and (c) the $1/x^2$ potential.

For the time-independent anharmonic potential, we compare our method with both shooting and annealing. In every case, we find our method to be advantageous over the two others, as regards both (a) cpu time required and (b) the ability of the method to find *all* paths connecting the two end points in a given time. Throughout this work we restrict ourselves to one dimension for simplicity in illustrating the method. Extension to more than one dimension is straightforward and, although no results are presented here, some test cases were done successfully and will be described in future work.

2. DISCRETIZED WKB PROPAGATORS FOR FAR-FROM-CAUSTIC AND NEAR-CAUSTIC CONDITIONS

In this section we derive the discretized expressions for the WKB propagator. The continuum forms are derived by Schulman [2].

The time evolution operator $U(t_n, t_0)$ for the (in general, time-dependent) Hamiltonian

$$H(t)=\frac{1}{2m}p^2+V(x,t), \tag{5}$$

with $p=m\dot{x}$, corresponding to the (in general, time-dependent) Lagrangian (3) can be written [14] as a product of short-time evolution operators over the interval t_n-t_0: $U(t_n,t_0)=U(t_n,t_n-\Delta t)\cdots U(t_0+\Delta t,t_0)$, where the short-time evolution operator is given in Ref. [14], $U(t+\Delta t,t)\approx 1-iH(t)\,\Delta t/\hbar\approx\exp(-iH(t)\,\Delta t/\hbar)$, where we neglect $O(\Delta t^2)$ terms. Inserting $(n-1)$ intermediate states we obtain for the propagator, K,

$$\begin{aligned}K(x_0,t_0;x_n,t_n)&=\langle x_n|U(t_n,t_0)|x_0\rangle\\&\approx\int dx_1\cdots dx_{n-1}\\&\quad\times\langle x_n|e^{-iH_{n-1}\Delta t/\hbar}|x_{n-1}\rangle\\&\quad\cdots\langle x_1|e^{-iH_0\Delta t/\hbar}|x_0\rangle,\end{aligned} \tag{6}$$

where t_0, t_n, and $\Delta t=(t_n-t_0)/n$ are, in general, complex and $H_j=H(t_0+j\,\Delta t)$. Equation (6) becomes exact in the limit $n\to\infty$, but for discretized numerical work we keep n large and finite. For $|\Delta t|$ sufficiently small, the Trotter approximation gives [2]

$$\begin{aligned}&\langle x_j|e^{-iH_{j-1}\Delta t/\hbar}|x_{j-1}\rangle\\&\quad\approx\frac{1}{\lambda}\exp\left[-\frac{m(x_j-x_{j-1})^2}{2i\hbar\,\Delta t}-\frac{i\,\Delta t}{2\hbar}(V_j+V_{j-1})\right],\end{aligned} \tag{7}$$

where $\lambda=(2\pi i\hbar\,\Delta t/m)^{1/2}$ is a quantity with dimension of length, and $V_j=V(x_j,t_0+j\,\Delta t)$.

For convenience, we introduce the free-particle reference path passing through the same end points, (x_0,t_0) and (x_n,t_n). In discretized form, this path, $\bar{x}(t_j)\equiv\bar{x}_j$, is given by

$$\bar{x}_j=[(n-j)\,x_0+jx_n]/n,\qquad j=0,\ldots,n, \tag{8}$$

and we now make the variable transformation, $y_j=x_j-\bar{x}_j$. We then find that (6) becomes

$$\begin{aligned}K(x_0,t_0;x_n,t_n)=\exp\Bigg[\frac{i}{\hbar}\Bigg(&\frac{m(x_n-x_0)^2}{2(t_n-t_0)}\\&-\frac{\Delta t}{2}(V_0+V_n)\Bigg)\Bigg]\tilde{K}(0,t_0;0,t_n),\end{aligned} \tag{9}$$

where the reduced propagator $\tilde{K}$ for propagating from $y_0=0$ to $y_n=0$ is given by

$$\tilde{K}(0,t_0;0,t_n)=\frac{1}{\lambda^n}\int dy_1\cdots dy_{n-1}\exp\left[\frac{i}{\hbar}\tilde{S}(\{y_j\})\right], \tag{10}$$

and the reduced action $\tilde{S}$ as a function of the discretized path is

$$\tilde{S}(\{y_j\})=\frac{m}{2\Delta t}\sum_{j=1}^{n}(y_j-y_{j-1})^2-\Delta t\sum_{j=1}^{n-1}V_j, \tag{11a}$$

$$=-\frac{m}{2\Delta t}t_{jk}\,y_j\,y_k-\Delta t\sum_{j=1}^{n-1}V_j. \tag{11b}$$

The notation $\{y_j\}$ is short for the whole set $y_1,\ldots,y_{n-1}$. In (11a), $y_0=y_n=0$ is understood and $V_j=V(y_j+\bar{x}_j, t_0+j\,\Delta t)$ is the potential, *shifted* in the y_j coordinate by $\bar{x}_j$. In (11b), the $(n-1)\times(n-1)$-dimensional matrix t_{jk} is tridiagonal, with $t_{jj}=-2$ and $t_{j,j\pm1}=1$. The summation on repeated indices runs over $j=1,\ldots,n-1$.

The error in the Trotter short-time propagator (7) is $O(\Delta t)$; despite this, the full propagator (9) becomes exact in the limit $\Delta t\to 0$, $n\to\infty$, with $n\,\Delta t=t_n-t_0$ (Makri and Miller [9]).

a. *Far-from-Caustic Condition*

For a stationary phase approximation to (10), we require those y_j for which (11) is stationary, i.e., classical paths in classically allowed regions, and nonclassical paths otherwise. The numerical prescription for getting these will be the subject of Section 3. There may be several such well-separated paths connecting the given end points, in which case (10) will have a contribution from each. Consider one such path, y_j^C. Then (11) can be expanded about it,

$$\tilde{S}(\{y_j^C+\delta_j\})=\tilde{S}_C+\tfrac{1}{2}\delta^2\tilde{S}_{jk}^C\delta_j\delta_k+O(\delta^3), \tag{12}$$

where $\tilde{S}_C$ and $\delta^2\tilde{S}_{jk}^C=\partial^2\tilde{S}/\partial y_j\partial y_k$ are evaluated at $y_j=y_j^C$. The linear term, involving $\delta\tilde{S}_j^C=\partial\tilde{S}/\partial y_j$, evaluated at $y_j=y_j^C$, vanishes because of the stationary condition. The matrix $\delta^2\tilde{S}_{jk}^C$ can be obtained by differentiating (11b),

$$\delta^2\tilde{S}_{jk}^C=-\frac{m}{\Delta t}t_{jk}-\Delta t\,V_j''^C\delta_{jk}, \tag{13}$$

where $V''=\partial^2V/\partial x^2$ and $V_j''^C=V''(y_j^C+\bar{x}_j,\,t_0+j\,\Delta t)$. No sum over j is implied in the last term $V_j''^C\delta_{jk}$, and δ_{jk} is the Kronecker delta. For purely real (or purely imaginary) Δt, $\delta^2\tilde{S}_{jk}^C$ is a nonsingular real symmetric matrix (times i for Δt pure imaginary) and is diagonalizable by an orthogonal matrix, call it U_{jk}. For general complex Δt, however,

$\delta^2\tilde{S}^C_{jk}$ is a nonsingular complex symmetric matrix (not Hermitian), but still diagonalizable.

The integrals in (10) can now be evaluated in the $\hbar \to 0$ limit by truncating (12) at the quadratic term [2], transforming from y_j to δ_j, and then to ξ_j with $\delta_j = U_{jk}\xi_k$. The final result upon evaluating (10) and substituting into (9) is

$$K(x_0, t_0; x_n, t_n) = \sum_C \left(\frac{m}{2\pi i\hbar \Delta_C}\right)^{1/2} \times \exp\left[\frac{i}{\hbar}\left(\frac{m(x_n - x_0)^2}{2(t_n - t_0)} - \frac{\Delta t}{2}(V_0 + V_n) + \tilde{S}_C\right)\right], \tag{14}$$

where $\sum_C$ denotes a sum over all the stationary values of $\tilde{S}$ except those discussed below, and

$$\Delta_C = \Delta t(-\Delta t/m)^{n-1} \det(\delta^2\tilde{S}^C_{jk}), \tag{15a}$$

$$= \Delta t \det\left[t_{jk} + \frac{(\Delta t)^2}{m} V_j''^C \delta_{jk}\right]. \tag{15b}$$

In (14), the essential ingredients are $\tilde{S}_C$ and Δ_C, which can be calculated easily using (11) and (15), respectively, once the y_j^C are known. Both quantities are independent of n in the limit $n \to \infty$. Expression (14) is a central result; it is the WKB form for the propagator for the far-from-caustic regions.

The sum over C contains all classical paths connecting (x_0, t_0) to (x_n, t_n) in the classically allowed regions and only those nonclassical paths which do not lead to an exponentially growing term in (14) as one varies the end points into the classically unallowed regions. As will be illustrated in Section 4, a classically unallowed region occurs beyond a caustic, and two nonclassical paths exist in this region, which have complex y_j despite the fact that the end points are real. The paths are related to each other by complex conjugation and, similarly, so are their corresponding complex actions, $\tilde{S}_C$, and also (see next paragraph) their complex Δ_C's. One path leads to an exponentially growing term and must be discarded. This term arises because of the asymptotic nature of the theory; terms in (14), when analytically continued to the classically unallowed region by varying t_n, say, may not be admissable due to Stokes lines in the complex t_n plane. A heuristic explanation of this will be given in Section 4.

The phase of $\Delta_C^{1/2}$ is to be taken as follows: On the classically allowed side of the caustic, the phase can be made explicit by writing $\Delta_C^{1/2} = |\Delta_C|^{1/2} \exp(i\nu_C \pi/2)$, where ν_C is the number of negative eigenvalues of $\delta^2\tilde{S}^C_{jk}$ in the definition (15) of Δ_C. It has been shown (Pechukas [9], Levit and Smilanski [9]) that ν_C is equal to the number of times the path C touches a caustic between its end points. (We are using here the geometric picture of a caustic as an envelope of a family of classical paths—see example (c) in Section 4.) The fact that Δ_C picks up a phase factor $e^{i\pi}$, after the allowed path C touches a caustic, can be made plausible by noting that an eigenvalue of $\delta^2\tilde{S}^C_{jk}$, λ_1 say, becomes zero when C ends on a caustic and changes sign after the end point of C moves away from the caustic after having touched it. Since Δ_C is proportional to the product of all the eigenvalues, the result follows. As the classical path is analytically continued past the caustic to the classically unallowed side by varying an end point, Δ_C becomes purely imaginary, since (typically) one of the eigenvalues of $\delta^2\tilde{S}^C_{jk}$, λ_1 say, becomes purely imaginary, and the remaining eigenvalues are purely real; hence, $\Delta_C^{1/2}$ picks up a phase factor $e^{i\pi/4}$, i.e., $\lambda_1 \to e^{i\pi/2}\lambda_1$, so that $\lambda_1^{1/2} \to e^{i\pi/4}\lambda_1^{1/2}$ and $\Delta_C^{1/2} \to e^{i\pi/4}\Delta_C^{1/2}$. The Δ_C's for the two nonclassical paths that emerge from a caustic on the classically unallowed side are related by complex conjugation, because these are the analytic continuations of the Δ_C's for the classical paths coalescing at the caustic, and the latter Δ_C's differ by a minus sign. This same choice of phase for $\Delta_C^{1/2}$ also enters the uniform asymptotic form where both nonclassical paths contribute (see Section 4).

b. *Near-Caustic Condition*

When the Δ_C becomes small for some classical path, the prefactor of (14) for that path blows up and we have the condition where the classical path is close to a caustic, i.e., the locus of points in the space of x_0, t_0, x_n, t_n such that two or more paths connecting (x_0, t_0) to (x_n, t_n) are coalescing. The WKB expression given in (14) is then a poor approximation to the actual propagator, so that we must derive a new approximation for the caustic region. An asymptotic matching of the WKB propagators in the classically allowed region, caustic region, and unallowed region will be required [15]. Alternatively, a uniform asymptotic approximation can be employed; this approximation is valid uniformly (i.e., equally for all regions), and, in particular, it interpolates between the far-from-caustic and near-caustic regions. We do not derive this form here (see [2, 18, 19]), but in Section 4 we present results for the uniform approximation for the $1/x^2$ potential.

Let y_j^C be a particular classical path which is near some caustic classical path y_j^F. We consider the case where x_0, t_0, x_n are the same for both paths C and F, but t_n^F is the final time for F, and t_n^C that for C, with difference $\tau = t_n^C - t_n^F$. We assume the usual case that the caustic occurs in purely real time so that t_0, t_n^F, and y_j^F are all real; however, t_n^C may be complex but near t_n^F. We also define the spatial difference between the two paths at each time slice, $\eta_j = y_j^C - y_j^F$; the two paths have the same total number of time slices, so that η_j is defined for each j.

First, the action along an arbitrary path y_j connecting t_0 and $t_n^C = t_n^F + \tau$ is expanded about t_n^F. We need not expand explicitly, but by using (11b), we can show directly that

$$\tilde{S}(\{y_j\}; t_0, t_n^F + \tau) - \tilde{S}(\{y_j\}; t_0, t_n^F) = -\chi E(\{y_j\}; t_0, t_n^F, \tau), \tag{16}$$

where $\chi = \tau/(t_n^F - t_0)$ and

$$E(\{y_j\}; t_0, t_n^F, \tau) = -\frac{m}{2\Delta t} t_{jk} y_j y_k + \left(\frac{t_n^F - t_0}{\tau}\right) \sum_{j=1}^{n-1} [\Delta t\, V(t_0 + j\,\Delta t) - \Delta t_F\, V(t_0 + j\,\Delta t_F)], \tag{17a}$$

where $V(t_0 + j\,\Delta t) = V(y_j + \bar{x}_j,\ t_0 + j\,\Delta t)$, $\Delta t = \Delta t_F + \tau/n$, and $\Delta t_F = (t_n^F - t_0)/n$. For V independent of t this reduces to

$$E(\{y_j\}; t_0, t_n^F, \tau) = -\frac{m}{2\Delta t} t_{jk} y_j y_k + \Delta t_F \sum_{j=1}^{n-1} V_j. \tag{17b}$$

To lowest order in τ, (17a) and (17b) are the integrals of the Hamiltonian with respect to time along a path y_j. Next, the action along the arbitrary path is expanded about y_j^F as follows:

$$\begin{aligned}\tilde{S}(\{y_j^F + \varepsilon_j\}; t_0, t_n^C) &= \tilde{S}(\{y_j^F + \varepsilon_j\}; t_0, t_n^F) \\ &\quad + [\tilde{S}(\{y_j^F + \varepsilon_j\}; t_0, t_n^F + \tau) \\ &\quad - \tilde{S}(\{y_j^F + \varepsilon_j\}; t_0, t_n^F)] \\ &= \tilde{S}(\{y_j^F + \varepsilon_j\}; t_0, t_n^F) \\ &\quad - \chi E(\{y_j^F + \varepsilon_j\}; t_0, t_n^F, \tau).\end{aligned} \tag{18}$$

Then we have

$$\tilde{S}(\{y_j^F + \varepsilon_j\}; t_0, t_n^F) = \tilde{S}_F + \tfrac{1}{2}\delta^2\tilde{S}_{jk}^F \varepsilon_j \varepsilon_k + \tfrac{1}{6}\delta^3\tilde{S}_{jkl}^F \varepsilon_j \varepsilon_k \varepsilon_l + O(\varepsilon^4), \tag{19}$$

where $\tilde{S}_F$, $\delta^2\tilde{S}_{jk}^F$, and $\delta^3\tilde{S}_{jkl}^F$ are defined similarly to $\tilde{S}_C$ and $\delta^2\tilde{S}_{jk}^C$ above, but evaluated along the caustic path F. The linear term vanishes because, for times t_0 and t_n^F, y_j^F is the classical path, which renders $\tilde{S}$ stationary. In a similar manner, we obtain

$$E(\{y_j^F + \varepsilon_j\}; t_0, t_n^F, \tau) = E_F + \delta E_j^F \varepsilon_j + \tfrac{1}{2}\delta^2 E_{jk}^F \varepsilon_j \varepsilon_k + \tfrac{1}{6}\delta^3 E_{jkl}^F \varepsilon_j \varepsilon_k \varepsilon_l + O(\varepsilon^4), \tag{20}$$

and the derivatives of E can be obtained from (17a) or (17b) in the same way as those for $\tilde{S}$ and are evaluated along the caustic path y_j^F.

Since we have assumed that the caustic occurs in pure real time, $\delta^2\tilde{S}_{jk}^F$ is real symmetric and is diagonalized by an orthogonal matrix, U_{jk}. The caustic condition implies that $\det(\delta^2\tilde{S}_{jk}^F) = 0$, so that at least one eigenvalue of $\delta^2\tilde{S}_{jk}^F$ is zero. We consider the usual case that one eigenvalue is zero, corresponding to $j = 1$, say, and the others are nonzero.

We break up ε_j into a contribution from the difference between y_j^C and y_j^F, namely $\eta_j = y_j^C - y_j^F$, plus the difference between the arbitrary path y_j and y_j^C, namely $\delta_j = y_j - y_j^C$, i.e., $\varepsilon_j = \eta_j + \delta_j$. With the further transformation from δ_j to ξ_j, where $\delta_j = U_{jk}\xi_k$, (18) becomes

$$\begin{aligned}\tilde{S} = &[(\tilde{S}_F + \tfrac{1}{2}\delta^2\tilde{S}_{jk}^F \eta_j \eta_k + \tfrac{1}{6}\delta^3\tilde{S}_{jkl}^F \eta_j \eta_k \eta_l) \\ &- \chi(E_F + \delta E_j^F \eta_j + \tfrac{1}{2}\delta^2 E_{jk}^F \eta_j \eta_k + \tfrac{1}{6}\delta^3 E_{jkl}^F \eta_j \eta_k \eta_l)] \\ &+ [(\delta^2\tilde{S}_{jk}^F \eta_k + \tfrac{1}{2}\delta^3\tilde{S}_{jkl}^F \eta_k \eta_l) \\ &- \chi(\delta E_j^F + \delta^2 E_{jk}^F \eta_k + \tfrac{1}{2}\delta^3 E_{jkl}^F \eta_k \eta_l)]\, U_{jm}\xi_m \\ &+ \tfrac{1}{2}[(\delta^2\tilde{S}_{jk}^F + \delta^3\tilde{S}_{jkl}^F \eta_l) \\ &- \chi(\delta^2 E_{jk}^F + \delta^3 E_{jkl}^F \eta_l)]\, U_{jm} U_{kn} \xi_m \xi_n \\ &+ \tfrac{1}{6}[\delta^3\tilde{S}_{jkl}^F - \chi\delta^3 E_{jkl}^F]\, U_{jm} U_{kn} U_{lp} \xi_m \xi_n \xi_p \\ &+ O(\varepsilon^4).\end{aligned} \tag{21}$$

The terms in the four square brackets can be identified with $\tilde{S}_C$, $\delta\tilde{S}_j^C$, $\delta^2\tilde{S}_{jk}^C$, and $\delta^3\tilde{S}_{jkl}^C$, respectively, and expanded about y_j^F and t_n^F to $O(\eta^3)$, $O(\eta^2)$, $O(\eta)$, and $O(1)$, respectively. If terms to all orders in η are included in the expansion of $\delta\tilde{S}_j^C$, it vanishes; but, in the spirit of the near-caustic asymptotic theory, higher order terms in η do not contribute in the $\hbar \to 0$ limit to the integration in (10). To identify the contributing terms it is sufficient to do an order of magnitude estimation of all the terms. Terms depending on ξ_j, i.e., all but the constant term, will contribute only if they are $O(\hbar)$ to cancel the $\hbar$ dividing $\tilde{S}$ in (10). For the purpose of estimating the order of magnitude of the terms, the $\tilde{S}$, E, and U matrices can be treated as $O(1)$, and $\tilde{S}$ can be roughly thought of as

$$\begin{aligned}\tilde{S} \sim \text{const} + \sum_{j=1}^{n-1} &\{[(\eta + \eta^2) - \chi(1 + \eta + \eta^2)]\, \xi_j \\ &+ [(\lambda_j + \eta) - \chi(1 + \eta)]\, \xi_j^2 + [1 - \chi]\, \xi_j^3\} \\ &+ \text{higher terms},\end{aligned} \tag{22}$$

where $\lambda_j = \delta^2\tilde{S}_{kl}^F U_{kj} U_{lj}$ are the eigenvalues of $\delta^2\tilde{S}_{jk}^F$. Since η is a measure of the deviation of our classical path from the caustic, we can examine $\tilde{S}$ for any size η. The near-caustic condition occurs when $\eta = O(\hbar^{2/3})$ [2], and hence τ and χ are $O(\hbar^{2/3})$. For $j = 1$, we have $\lambda_1 = 0$, and the leading contributions to (10) come from $\chi\xi_1$, $\eta\xi_1$, and ξ_1^3, with $\xi_1 = O(\hbar^{1/3})$. Then all the other ξ_1 terms are of higher power in $\hbar$ and have a vanishing contribution as $\hbar \to 0$. For $j \neq 1$,

we have $\lambda_j = O(1)$, and the leading contribution comes from $\lambda_j \xi_j^2$ with $\xi_j = O(\hbar^{1/2})$; the other ξ_j terms are of higher order.

Hence, with only the contributing terms explicit, (21) becomes

$$\tilde{S} = \tilde{S}_C + v\xi_1 + \tfrac{1}{3}u\xi_1^3 + \tfrac{1}{2}\sum_{m=2}^{n-1} \lambda_m \xi_m^2 + \text{noncontributing terms}, \tag{23}$$

where

$$v = (\delta^2 \tilde{S}_{jk}^F \eta_j - \chi \delta E_k^F)\, U_{k1} = -\chi \delta E_k^F U_{k1}. \tag{24a}$$

Note that $\delta^2 \tilde{S}_{jk}^F U_{k1}$ is zero for all j, since U_{k1} is the eigenvector of $\delta^2 \tilde{S}_{jk}^F$ with zero eigenvalue. Explicitly, for V time-independent, we have

$$v = \chi \left[\frac{m}{\Delta t} t_{jk} y_j^F - \Delta t_F V_k'^F \right] U_{k1}, \tag{24b}$$

and a similar expression for V time-dependent. Also, we have

$$u = \tfrac{1}{2}\delta^3 \tilde{S}_{jkl}^F U_{j1} U_{k1} U_{l1}, = -\tfrac{1}{2} \Delta t_F V_j'''^F U_{j1}^3. \tag{25}$$

Substituting into (10), we find the integrations over ξ_j, $j \neq 1$, can be done as in the far-from-caustic case; the integration over ξ_1 yields the Airy function, Ai(z). The result upon integrating is the following contribution to $K(x_0, t_0; x_n, t_n)$:

$$\frac{m}{i\hbar^{2/3}(\Delta_F u^{2/3})^{1/2}} Ai\left(\frac{v}{u^{1/3}\hbar^{2/3}}\right) \times \exp\left[\frac{i}{\hbar}\left(\frac{m(x_n - x_0)^2}{2(t_n - t_0)} - \frac{\Delta t}{2}(V_0 + V_n) + \tilde{S}_C\right)\right], \tag{26}$$

where

$$\Delta_F = (\Delta t)^2 (-\Delta t/m)^{n-2} \det'(\delta^2 \tilde{S}_{jk}^F), = (\Delta t)^2 (\Delta t/\Delta t_F)^{n-2} \det'\left[t_{jk} + \frac{(\Delta t_F)^2}{m} V_j''^F \delta_{jk} \right], \approx (\Delta t_F)^2 \det'\left[t_{jk} + \frac{(\Delta t_F)^2}{m} V_j''^F \delta_{jk} \right] \tag{27}$$

and det' means the product of all the eigenvalues with the zero eigenvalue removed. We set $(\Delta t)^2 (\Delta t/\Delta t_F)^{n-2} \approx (\Delta t_F)^2$, since we take the limit $\hbar \to 0$ with n fixed, and we recall $\Delta t - \Delta t_F = \tau/n = O(\hbar^{2/3})$. It is important to note that this approximation, together with that made in neglecting terms in (21), is valid in the strict limit $\hbar \to 0$, and for the values of $\hbar$ and n used in practice, one appears to find large corrections to the u, v, and Δ_F terms retained. However, because of the asymptotic nature of the theory, including such corrections in the exponential gives *poorer* agreement with the exact result. The correction due to these terms can be obtained by expanding the exponential containing them in a Taylor series and by treating the resulting series after integration as an asymptotic one.

Expression (26) is to replace those terms in (14) for paths within $O(\hbar^{2/3})$ of a caustic path; however, on both the classically allowed and unallowed sides, there are two coalescing paths at the caustic, and the actions for the two are equal only at the caustic. The action entering (26) can be the action for either path; but, to increase the range over which (26) is valid, one can take the contribution from each path as follows: On the classically allowed side, each classical path contributes one-half of (26). To keep the phase relation between these two terms correct, one replaces Δ_F by $p\Delta_F$, where p is the phase, i.e., + or −, of the eigenvalue of $\delta^2 \tilde{S}_{jk}^C$ which vanishes at the caustic. Then the sign of $p\Delta_F$ agrees with the sign of Δ_C, and the phase of $(p\Delta_F)^{1/2}$ in (26) is chosen as for $\Delta_C^{1/2}$ (see discussion above). On the classically unallowed side, one must take just the one term, (26), corresponding to the path whose action does not lead to an exponentially growing term in (26). On the classically unallowed side, the phase of $\Delta_F^{1/2}$ is chosen as described for $\Delta_C^{1/2}$ in the preceding section. Other paths which may exist for the given set of end points, but are not coalescing at the caustic under discussion, contribute as in (14).

Expression (26) is analogous to that of Eq. (15, 16) of Schulman [2], but with the following differences: (a) our result is for the discretized case, whereas Schulman gives the result for the continuous case; (b) we approach the caustic by varying t_n, whereas Schulman approaches it by varying x_n; as a result our expression (24) for v differs from his; (c) we give an explicit computable algorithm for the square-root prefactor in (26), whereas Schulman leaves the prefactor indeterminate with form 0/0 on the caustic; (d) Schulman does not bother to calculate all the factors preceding Ai(z) in (26); these factors are needed for our later applications.

The essential ingredients in (26) are $\tilde{S}_C$, Δ_F, v, and u, and are easily calculated once y_j^C and y_j^F are known. If U_{j1} is normalized such that $\sum_{j=1}^{n-1} U_{j1}^2 = 1$, then $\Delta_F \sim n$, $v \sim n^{-1/2}$, and $u \sim n^{-3/2}$ as $n \to \infty$, but (26) is independent of n as $n \to \infty$. Since U_{j1} is an eigenvector, it contains an ambiguous overall phase, i.e., + or −; however, this ambiguity drops out of (26). In the argument of the Airy function, both v and u are odd in U_{j1} and, since the principal root is to be taken in calculating $u^{1/3}$, the argument is independent of the phase of U_{j1}. In the prefactor, $u^{2/3} = (u^{1/3})^2$ is always positive and hence is independent of the phase of U_{j1}; the principal root

in $(u^{2/3})^{1/2}$ is taken. The sign of v is also determined by the sign of χ, which depends on $t_n^C - t_n^F$ and therefore changes in crossing the caustic.

3. THE RELAXATION METHOD FOR THE CLASSICAL PATHS

In this section we formally present our relaxation method for obtaining the classical path as a function of end points. By making the variable transformation from x_j to y_j, the equivalent problem is to obtain the classical path in the y_j coordinate, where the boundary condition is always $y_0 = y_n = 0$, with the same times t_0, t_n as for x_j. The difference in the boundary conditions is absorbed into the shift in the potential.

The principle of least action states that (11) is stationary for the classical paths, which are therefore solutions to

$$\frac{\partial \tilde{S}}{\partial y_j} = \delta \tilde{S}_j = -\frac{m}{\Delta t} t_{jk} y_k - \Delta t \, V_j' = 0, \tag{28}$$

where $V' = \partial V / \partial x$ and $V_j' = V'(y_j + \bar{x}_j, t_0 + j \, \Delta t)$. Note that, in general, V_j' depends on y_j nonlinearly, so that (28) is a nonlinear algebraic equation for y_j. This nonlinearity renders (28) nontrivial to solve, but, in compensation, yields some interesting physics, i.e., the possibility of more than one solution, corresponding to the possibility of more than one path connecting the given end points. To solve (28) we employ a Newton–Raphson (NR) technique in the $(n-1)$-dimensional space of y_j. The NR approximation to the vector Δy_j, which points from a starting point of arbitrary y_j to the solution of (28), is

$$\Delta y_j = -[\delta^2 \tilde{S}_{jk}]^{-1} \, \delta \tilde{S}_k \tag{29a}$$

$$= -\left[t_{jk} + \frac{(\Delta t)^2}{m} V_j'' \delta_{jk} \right]^{-1} \left[t_{kl} y_l + \frac{(\Delta t)^2}{m} V_k' \right], \tag{29b}$$

where V_j' and V_j'' are evaluated at the current values of y_j. The numerical procedure, then, is to start at some *good* guess for y_j^C and iterate according to $y_j^{\text{new}} = y_j^{\text{old}} + \Delta y_j$, until the method converges to y_j^C. At first sight the numerical effort seems bigger than it actually is, because one has to invert an $(n-1) \times (n-1)$ matrix for each iteration. However, this matrix is tridiagonal, with complex diagonal terms, in general, and unit near-diagonal terms. Inversion and multiplication by the rightmost vector in (29b) can be done by Gaussian elimination plus back substitution (GEB) and is an order n operation [16]. A similar scheme can be employed to calculate the determinant in (15b) for the far-from-caustic expression. With the matrices set exactly as displayed in (15b) and (29b), GEB involves only differences between numbers of order n, except near a caustic. With n set to a reasonable value, $n \approx 100$, this poses no numerical problem. One can see this point by taking the simple case where $V = 0$. Then the determinant in (15b) is equal to n.

Some difficulty can arise near a caustic. Then the matrix to be inverted in (29b) becomes singular. Owing to the particularly simple form of the cubic term in the expansion of $\tilde{S}$, a higher order NR can be employed to avoid this singularity, but for the cases studied here we were able to achieve remarkably good results without this. If the *zero eigenvalue* at the caustic is taken as small, say $\sim 10^{-6}$, which is still numerically viable in GEB, then the convergence is to within the region of error between the actual and discretized path for $n \approx 100$. However, if the choice of x_0, t_0, x_n, t_n (with t_0, t_n purely real) puts an end point sufficiently past a caustic into a classically unallowed region, the method does not converge. Since convergence occurs typically in less than 10 to 20 steps for $n \approx 100$, if the method does not converge after 20 steps, one can assume that the path lies sufficiently in a classically unallowed region.

To obtain the nonclassical paths on the classically unallowed side one can *trace* a path's evolution around the caustic in complex time and back to classically unallowed real times. A path's evolution is *traced* by varying x_0, t_0, x_n, t_n slowly (in this case only t_n) using y_j^C from the previous path as the initial guess for the next. The procedure then is to approach the caustic in real time, add a small imaginary time (of either sign), increase (or decrease) the real part of the time past the caustic time, and then subtract the imaginary time part. As will be illustrated in Section 4, a generic caustic involves two classical paths coalescing into one. Two nonclassical paths survive past the caustic in complex y_j and real t_0, t_n, and each can be arrived at by tracing either coalescing classical path around the caustic in both positive and negative imaginary time. These paths are related to each other by complex conjugation.

Related to this is the question of obtaining *all* the classical paths connecting a particular set of end points. Since the relaxation method converges on only one path at a time, one is not sure of the existence of other paths. The procedure to obtain other classical paths is to follow one classical path, obtained by the relaxation method starting from an initial guess, to a caustic by varying x_n or t_n. To obtain the second classical path coalescing with the first at the caustic, one need only trace the first path once completely around the caustic in complex time back to classically allowed real times. This classical path then evolves into the other classical path at the caustic, which can in turn be traced to other caustics and the process repeated. In this way, all the paths in x_0, t_0, x_n, t_n can be mapped out. This point is illustrated in Section 4 with the anharmonic potential, where the classical paths are not known analytically, and a heuristic explanation for why this works is given there.

Thus far we have all the necessary numerical tools for the far-from-caustic WKB form and for the uniform

approximation presented in Section 4. We next consider the near-caustic form. Once a classical path is found in which Δ_C is $O(\hbar^{1/3})$, i.e., one eigenvalue of $\delta^2\tilde{S}^C_{jk}$ is $O(\hbar^{1/3})$ and the rest are $O(1)$, Eq. (14) is becoming a poor approximation and one should switch to (26). For this, the nearby caustic path must first be found by varying t_n until Δ_C is below some tolerance. In practice, if the propagator is to be found several times, this effort is not wasted because each classical path obtained in approaching the caustic path can be used in a near-caustic WKB propagator. Once the caustic path is found, a diagonalization of $\delta^2\tilde{S}^F_{jk}$ can be done by a QL algorithm with implicit shifts [17]. If one deals with $(-m/\Delta t_F)\,\delta^2\tilde{S}^F_{jk} = t_{jk} + (\Delta t_F)^2\, V_j''^F \delta_{jk}/m$, rather than $\delta^2\tilde{S}^F_{jk}$, then one is again in the situation where the algorithm deals only with numbers of order n. This procedure for obtaining the eigenvalues and eigenvectors is an order n^3 operation, and so it is slower than what is required for the far-from-caustic WKB form. However, once these are known, they can be used to construct all the near-caustic WKB propagators for near-caustic paths with fixed x_0, t_0, x_n. The quantities u and v depend on the near-caustic path in a trivial way and can by obtained by an order 1 operation. On a Sun Sparc station 1, one thousand paths can be obtained in 35 s of cpu time, while diagonalizing $\delta^2\tilde{S}^F_{jk}$ takes 14 s for $n = 100$.

4. ILLUSTRATIONS OF THE RELAXATION ALGORITHM

In this section, we implement our relaxation algorithm for three examples. The intention here is to illustrate the algorithm's ability to deal with Lagrangians of the general form (3) in obtaining the action and other quantities discussed in Section 2, via the classical path. A complete comparison of exact and WKB propagators for the $1/x^2$ potential will be presented elsewhere [18].

The examples considered are: (a) a harmonic potential with time varying equilibrium position; (b) a double-well anharmonic potential; and (c) the repulsive $1/x^2$ potential. For the last example, the paths and action are known analytically as functions of end points, so that a more extensive check can be made than in the previous examples.

a. *The Time-Dependent Harmonic Potential*

The relaxation algorithm is particularly adept for quadratic Lagrangians of the most general form, because in this case $\delta^2\tilde{S}_{jk}$ is independent of y_j and the method converges in one iteration; hence the algorithm has an obvious advantage over shooting methods, which require at least three iterations for convergence.

Quadratic Lagrangians (which include linear potentials and free particles as special cases) are unique in that there is only one path for a given set of end points, except at a caustic, where there are infinitely many paths. The latter case corresponds to δ-function focusing of the propagator. The propagator is given exactly by (14) in all cases.

We consider the following example, taking

$$V_j = \tfrac{1}{2}k(y_j - \bar{y}_j)^2,$$
$$\bar{y}_j = \sigma[j \bmod (n/2)]/n, \tag{30}$$

where *mod* gives the remainder after integer division of j by $(n/2)$. This potential represents a harmonic oscillator whose equilibrium position moves with constant velocity in the positive y direction, but suddenly snaps back to $y = 0$ half way through the time interval, $t_n - t_0$. Some examples of paths in purely real and purely imaginary time, for $n = 100$, are shown in Figs. 1a, b. We measure mass, time, and length in units of m, $(m/k)^{1/2}$, and σ, respectively. A check that, for the relaxation algorithm, the energy remains constant along the two legs of the path, i.e., $j < n/2, j > n/2$, shows that, for

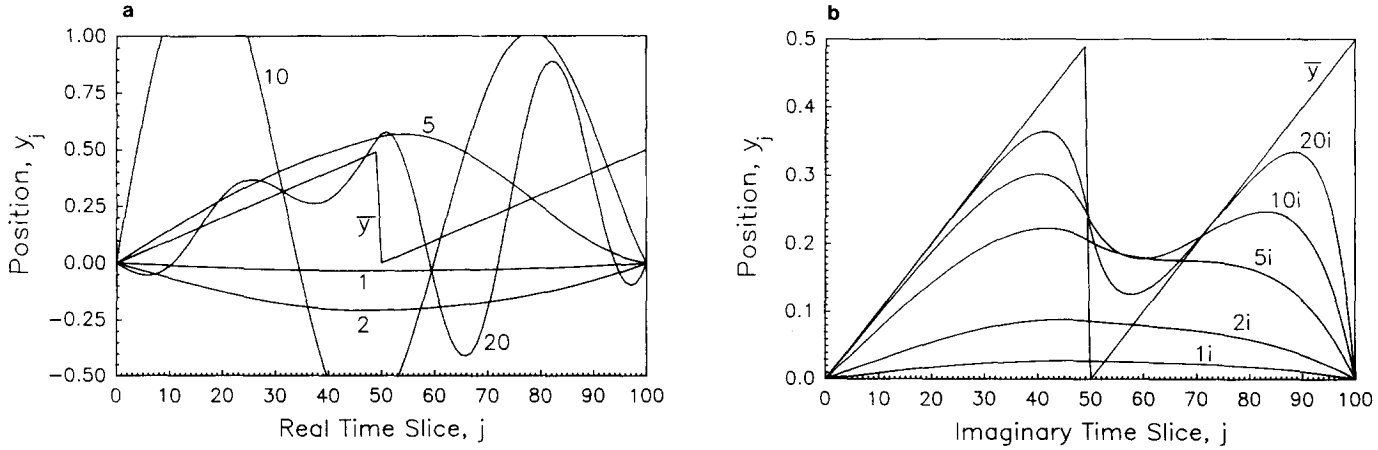

FIG. 1. Classical paths for the harmonic potential with time varying equilibrium position. The numbers labeling the paths indicate the time $t = t_n - t_0$ to travel from $y_0 = 0$ to $y_n = 0$, and the curve labeled $\bar{y}$ is the equilibrium position.

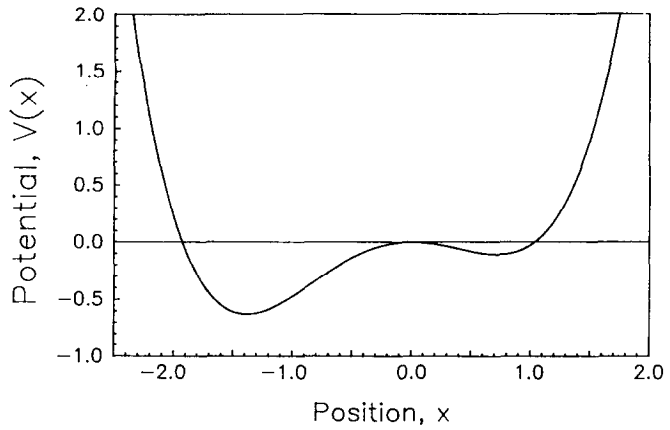

FIG. 2. The asymmetric double-well anharmonic potential.

$t = 10$, the largest deviation from the average energy is 3.1, 2.4, 1.0, and 0.5% for $n = 100$, 200, 500, and 1000, respectively.

b. *The Anharmonic Potential*

A more interesting example is the asymmetric double-well anharmonic potential, $V(x) = C[(x/\sigma)^4/4 + 2(x/\sigma)^3/9 - (x/\sigma)^2/2]$, depicted in Fig. 2. We measure mass, time, and length in units of m, $\sigma(m/C)^{1/2}$, and σ, respectively. Owing to the rich structure of the paths, we illustrate only classical paths in real time and concentrate on those paths in the well bounded by $x = -2$ and $x = 0$. For any set of end points, there are infinitely many paths, almost all of which are high energy paths bouncing many times off the hard x^4 walls. Such paths contribute little to the sum over classical paths in (14), since Δ_C turns out to increase with the number of bounces, and large Δ_C suppresses the contribution. We do not consider these paths because of their relatively simple structure. A check that, for the relaxation algorithm, the energy remained constant along the paths we consider shows that the largest deviation from the average energy is 5.0% for $n = 100$ in the worst case; for $n > 100$ the error in the energy is reduced, as in Section a.

Of greater interest is the existence of several paths for one set of end points and their evolution as they are traced up to a caustic, varying $t = t_n - t_0$ or x_n. For $x_0 = x_n = -1$ and $t = 10$, eight classical paths exist which remain within the bounds $x = -2$ and $x = 0$. Figure 3a depicts three of the four *even* paths at $t = 10$, 7.76, 6.83. (*Even* implies that the path reflects into itself when the path is reflected about its midpoint in time.) We label the most oscillatory path number 1, the least oscillatory number 3, and the other number 2. The one not shown we label number 4. Figure 3b depicts two of the four *uneven* paths for $t = 10$, 8.5, 7.76. The most oscillatory is labeled number 5, the other number 6. Paths 7 and 8 can be obtained from 5 and 6 by letting $j \to n - j$ (i.e., reflecting about the midpoint in time).

The best illustration of the advantage of the relaxation method over the shooting method can be made in terms of these paths. In every case when one is reasonably close to a path (in relaxing this means a reasonable initial guess to the whole path; in shooting, this means a reasonable initial guess to the initial velocity) we find that shooting takes six to 20 times more iterations than relaxing. To obtain comparable accuracy for the path and action by the two methods, we employ the fourth-order Runge–Kutta integration scheme for shooting, where one iteration of this method takes twice as much cpu time as one relaxation iteration.

However, this is not the greatest disadvantage of shooting; the greatest disadvantage lies in obtaining a path from its initial velocity when the nature of the path is such that it is fairly sensitively dependent on initial conditions. (It need not be chaotic.) In Figs. 3a and b it is clear that Paths

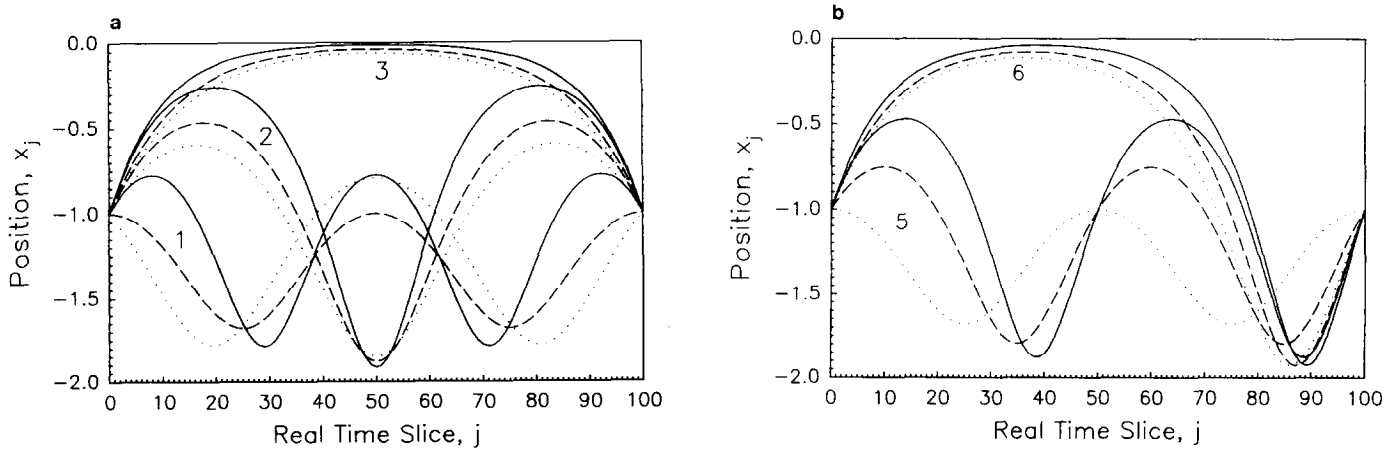

FIG. 3. Paths for the anharmonic potential: (a) Classical paths connecting $x_0 = x_n = -1$ in times $t = 10$ (solid lines), $t = 7.76$ (dashed lines), and $t = 6.83$ (dotted lines), for the even paths. Only paths 1, 2, 3 of the four even paths are shown. (b) Classical paths connecting $x_0 = x_n = -1$ in times $t = 10$ (solid lines), $t = 8.5$ (dashed lines), and $t = 7.76$ (dotted lines), for the uneven paths. Paths 7 and 8 are obtained from 5 and 6, respectively, by letting $j \to n - j$.

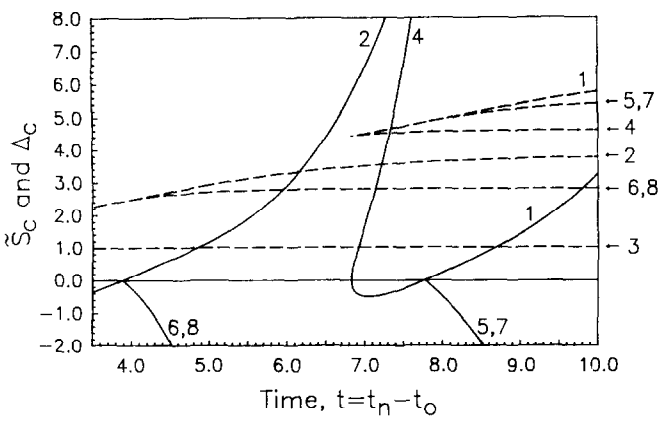

FIG. 4. The evolution of $\tilde{S}_C$ (dashed lines) for Paths 1, ..., 8 and Δ_C (solid lines) for Paths 1, 2, 4, 5, 7 as $x_0 = x_n = -1$ are kept fixed, and $t = t_n - t_0$ is varied. A path reaches a caustic when $\Delta_C = 0$.

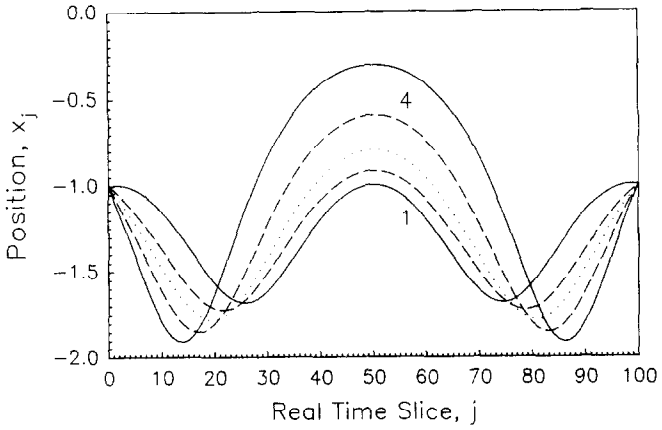

FIG. 5. The approach of Paths 1 and 4, with $x_0 = x_n = -1$ fixed, to the caustic path at $t = 6.83$ (dotted line). The paths shown are at $t = 8.0$ (solid lines) and $t = 7.0$ (dashed lines).

2, 3, 5, and 6 begin with similar velocities, and these initial velocities approach one another more closely as t is made larger. For $t = 10$, the initial velocities are $v_0 = 0.934005$, 0.971747, 0.837013, and 0.971141 for Paths 2, 3, 5, and 6, respectively. In order to distinguish Paths 3 and 6, one requires accuracy to the fourth digit in v_0. A similar problem is seen for Path 3 when one considers keeping time t fixed, but the end point x_n is varied. When Path 3 connects $x_0 = -1$ to $x_n = -1$ with $t = 10$, the initial velocity is $v_0 = 0.971747$, and when Path 3 connects $x_0 = -1$ to $x_n = -1.8$ with $t = 10$, the initial velocity is $v_0 = 0.971657$. The sensitive dependence on v_0 is again apparent, with five-figure accuracy in v_0 required to distinguish the two paths. For Path 3, this accuracy is required for shooting from $x_0 = -1$ to any x_n over the range $x_n = 0$ to $x_n = -1.9$, with time $t = 10$. Although paths may correspond to well-distinguished extrema of $\tilde{S}(\{y_j\})$, they may, and often do, have very close initial velocities. Since relaxation is based on finding these well-separated extrema, it does not suffer from having to distinguish paths by initial velocities, as shooting does. Thus, in contrast with our relaxation method, the shooting method will have difficulties in finding *all* paths connecting two end points.

We also obtained Paths 1, ..., 8 by the Doll *et al.* [11] simulated annealing method and found that this method takes at least 10^3 times as much cpu time to obtain a path, compared to our relaxation method, when one demands comparable accuracy. The stochastic procedure required in the method makes it uncompetitive with our method. Because Doll *et al.* do not discuss how to systematically obtain *all* the paths by their method, we found it necessary, in order to obtain all eight paths, to start annealing from good initial guesses for the paths, guided by the results obtained from our method.

The time evolution of $\tilde{S}_C$ for these eight paths, and the evolution of Δ_C for Paths 1, 2, 4, 5, 7, are shown in Fig. 4. Path 1 undergoes two caustic coalescences, at $t = 7.76$ and $t = 6.83$. The caustic coalescence at $t = 6.83$ involves the coalescence of Paths 1 and 4, and beyond this time lies the classically unallowed region for these paths. The approach of Paths 1 and 4 to the caustic path is shown in Fig. 5. This topological coalescence between the stationary action paths occurs because in the space of ξ_j (the space in which $\delta^2 \tilde{S}^C_{jk}$ is diagonal) a maximum annihilates a minimum along some direction, ξ_1, say, as t is varied. This is schematically shown in Fig. 6a and is the caustic condition considered in Section 2. However, the caustic coalescence at $t = 7.76$ is topologically different. In this case, three paths, 1, 5, and 7, come together and only one path, call it Path 1, survives as t is decreased. The same type of caustic coalescence occurs involving paths 2, 6, and 8 at $t = 3.89$ with path 2, say, surviving. In the space of ξ_j, this caustic occurs because along the ξ_1 direction, two minima and a maximum combine as t is decreased to form one minimum. This is schematically shown in Fig. 6b and is not the caustic situation considered in Section 2; that theory is not applicable for this topologically different caustic. However, the former case is generic whereas the latter is not. In the 3D space of x_0, x_n, t, the caustics form 2D manifolds which can intersect (along planes of symmetry) and form 1D lines. The nongeneric caustic occurs along these lines. In this example, when $x_0 = x_n$, reflecting a path about the midpoint in time leaves $\tilde{S}_C$ and Δ_C invariant. This symmetry gives rise to the nongeneric caustic along the line defined by $x_0 = x_n$ and $t = t_F$, where t_F is a single-valued function of x_0. If $x_0 \neq x_n$, we are no longer on this line and the nongeneric caustic does not occur. For example, for $x_0 = -1$ and $x_n = -1.2$, Path 5 coalesces with Path 4 at $t = 6.51$, and Path 7 coalesces with Path 1 at $t = 8.37$. The nongeneric caustic splits into two generic caustics. Still higher symmetries can give rise to yet other topologically distinct caustics which occur at points in x_0, x_n, t. An example of such a caustic, not considered here, occurs when $x_0 = x_n = 0$ for a symmetric double-well potential.

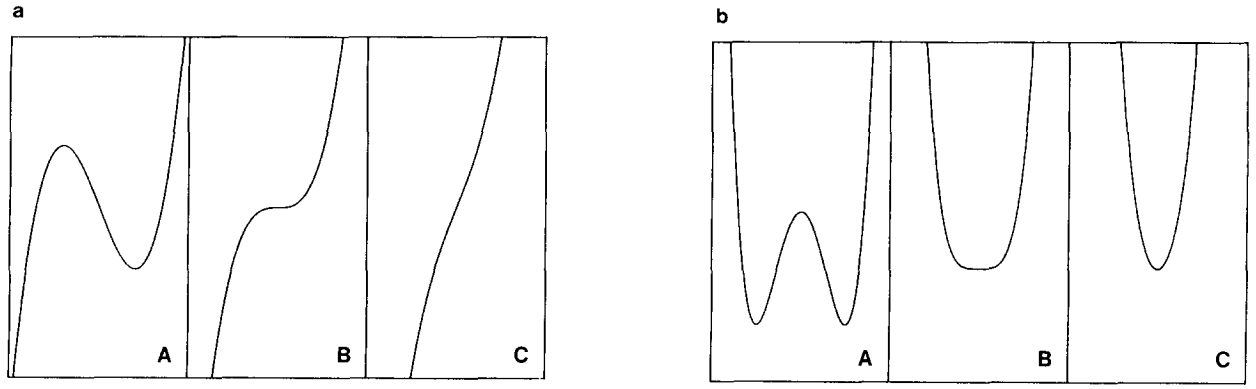

FIG. 6. The (a) generic and (b) nongeneric causting conditions. The frames show the action as a function of the coordinate ξ_1 (see text) along which the stationary values coalesce; (A) before, (B) while, and (C) after they coalesce.

A heuristic understanding of why one classical path coalescing at a caustic evolves into the other coalescing classical path, when traced around the caustic in complex time, can be obtained by considering the generic caustic depicted in Fig. 6a. As a function of ξ_1, the action behaves as $\tilde{S} \sim \xi_1^3 - a\xi_1$ and has stationary values at $\xi_1 = \pm\sqrt{a/3}$. Now the evolution of frames A, B, and C in Fig. 6a corresponds to $a > 0$, $a = 0$, $a < 0$, respectively, and a can be identified as being proportional to $\pm(t - t_F)$ for $|t - t_F|$ small. The + sign is taken if $t > t_F$ is the classically allowed region; otherwise, the − sign is taken. Then tracing once around the caustic corresponds to $a \to ae^{i2\pi}$, and hence $\sqrt{a/3} \to -\sqrt{a/3}$ and vice versa. The classical paths evolve into each other, and hence the stationary values of $\tilde{S}$ do as well. This argument also gives some understanding of the Stokes phenomenon and why the classical and nonclassical paths contribute as we describe in Section 2. On the classically unallowed side, $a < 0$ and two stationary values exist and lie at $\xi_1 = \pm i\sqrt{|a|/3}$; correspondingly, two nonclassical paths exist in complex y_j and are related to each other by complex conjugation. To obtain the contribution to the propagator for these stationary values in the action in the limit $\hbar \to 0$, the contour of integration for ξ_1 can be deformed only into the upper complex ξ_1 plane, and one obtains a contribution from just one nonclassical path by a Laplace argument on the deformed contour. On the classically allowed side, we have $a > 0$, and the two stationary points are on the real axis. The integration over ξ_1 then yields contributions from both stationary values by a stationary phase argument. This argument breaks down when $a = O(\hbar^{2/3})$ (the caustic condition), in which case taking $\hbar \to 0$ does not serve to localize the contribution of the integrand on the contour to just the neighbourhoods of the two stationary phase points in the classically allowed case, or to just the neighbourhood of the one stationary phase point in the classically unallowed case.

Paths can also coalesce at caustics by varying x_n at fixed t_n. Figure 7 shows the evolution of S_C for all eight paths and Δ_C for paths 1, 2, 4, 5, 7 as x_n is varied. All the caustics depicted are generic. Paths 5 and 7 (also 6 and 8) are not related by reflecting about the midpoint in time when $x_0 \neq x_n$, and the degeneracy seen in Fig. 4 is removed.

The maps of S_C (or $\tilde{S}_C$) and Δ_C in Figs. 4 and 7 are produced by tracing any one classical path to and around its caustics to the other classical paths we consider, i.e., those lying in $-2 < x < 0$. However, these paths also trace to other classical paths lying outside the range $-2 < x < 0$ and, in fact, we were not able to find any classical paths which did not trace to all the others. It is unclear if it is always possible to trace to all other classical paths in x_0, x_n, t from only one.

c. *The* $1/x^2$ *Potential*

For the repulsive potential $V(x) = C/x^2$, with $C > 0$, the paths, action, and exact propagator are known analytically

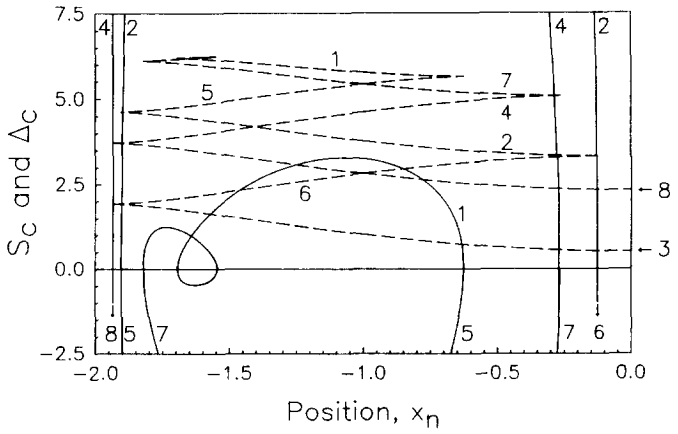

FIG. 7. The evolution of S_C (dashed lines) for Paths 1, ..., 8 and Δ_C (solid lines) for Paths 1, 2, 4, 5, 7 as $x_0 = -1$ and $t = 10$ are kept fixed and x_n is varied. Note that, to avoid cluttering the figure, two paths are unlabeled, between $x = -1.83$ and $x = -1.56$. The Δ_C curves for Paths 6 and 8 are not fully shown. They continue in the direction of the arrows. Path 6 connects to 3, and Paths 3 and 8 connect to paths lying outside $-2 < x < 0$.

as functions of x_0, x_n, and $t = t_n - t_0$. There are exactly two classical or nonclassical paths for all x_0, x_n, t, except those values corresponding to the caustic, where there is one path for each x_0, x_n, t; this caustic separates the classical and nonclassical regions along a ruled surface, with the classical region given by $x_0 x_n > \gamma t$, where $\gamma = (2C/m)^{1/2}$. For a given x_0, the caustic is the line, in the (x_n, t) space–time plane, defined by $x_n = \gamma t / x_0$; i.e., this line is the envelope for the family of paths emanating from x_0 with various initial velocities.

On the classically allowed side, usually one of the two paths is direct and the other indirect; i.e., one path (the direct one) does not have a turning point between the end points, whereas the other path (indirect) has one. For conditions where both paths are indirect, e.g., near the caustic or when $x_n = x_0$, we continue to use the label D for the path of lower action, and I for the path of higher action. Equivalently, one distinguishes the D and I paths from the property that a D path does not touch the caustic (envelope) between its end points, whereas an I path does. On the classically unallowed side, paths D and I are the analytic continuations of the paths D and I, respectively, from the classically allowed side.

The action for these paths is

$$S_C(x_0, x_n, t) = \frac{m}{2t}\left(x_0^2 + x_n^2 \pm 2(x_0^2 x_n^2 - \gamma^2 t^2)^{1/2}\right) \pm m\gamma(\sin^{-1}(\gamma t / x_0 x_n) - \lambda_{\pm}\pi), \quad (31)$$

where the $-$ sign corresponds to the *direct* path (D) for which $\lambda_- = 0$, and the $+$ sign corresponds to the *indirect* path (I) for which $\lambda_+ = 1$. For the value of $\sin^{-1}$, one takes the principal angle. In analytically continuing to the classically unallowed side, one must be careful in choosing the branch of the square root and $\sin^{-1}$ in (31). The exact propagator is [2]

$$K(x_0, x_n, t) = \left(\frac{m(x_0 x_n)^{1/2}}{i\hbar t}\right) \times \exp\left[\frac{im(x_0^2 + x_n^2)}{2\hbar t}\right] I_\nu\left(\frac{m x_0 x_n}{i\hbar t}\right), \quad (32)$$

where I_ν is the modified Bessel function of index $\nu = \frac{1}{2}(1 + 8mC/\hbar^2)^{1/2}$. We measure mass, time, and length in units of m, $\sigma^2(m/C)^{1/2}$, and σ, respectively, where σ is an arbitrary length scale. A check that, for the relaxation algorithm, the energy remains constant along the paths we consider, shows that $n = 100$ is sufficiently large to give good results.

For $n = 100$, there is remarkably good agreement between the exact and discretized quantities. With the exceptions discussed below, the discretized paths, S_C and Δ_C are within 0.1 % of the exact values. Figure 8 depicts both paths, D and I, for $x_0 = 3$, $x_n = 4$, and $t = 5 + 0i$, $3 + 4i$, $0 + 5i$. Path I for $t = 0 + 5i$ is interesting, since it runs into the singularity of the potential in finite imaginary time (as it does for any pure imaginary time). The algorithm makes its largest error when the path is deepest within the potential, with maximum relative error in the path $\sim 100\%$ at $j = 30, 57$; however, the absolute error is small and S_C and Δ_C are still within 0.1 % of the exact values. A similar error occurs for path I for real times when $t \to 0$ and the path runs deep within the potential, but S_C and Δ_C remain quite accurate.

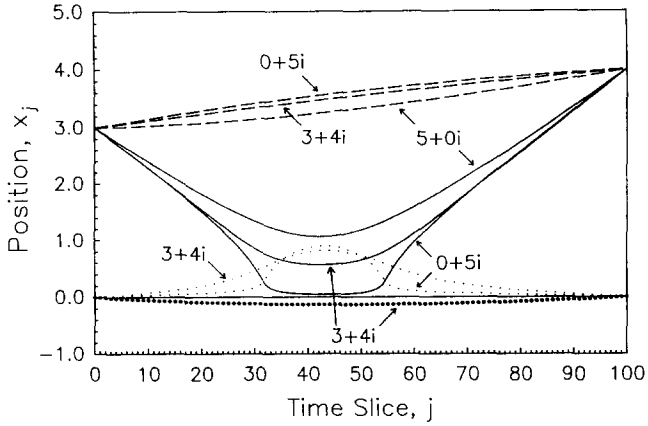

FIG. 8. Paths for the $1/x^2$ potential; Paths I (solid lines for the real part, light dotted lines for the imaginary) and Paths D (dashed lines for the real part, heavy dotted lines for the imaginary) connecting $x_0 = 3$ to $xn = 4$ in times $t = 5 + 0i$, $3 + 4i$, and $0 + 5i$. For $t = 5 + 0i$ and $0 + 5i$, Path D is purely real, while Path I is purely real only for $t = 5 + 0i$.

For the paths connecting $x_0 = 3$ and $x_n = 4$ in real classically allowed and unallowed times, S_C and Δ_C are plotted in Fig. 9. Beyond $t_F = 8.485$, S_C for both paths is complex, and the two values are related to each other by complex con-

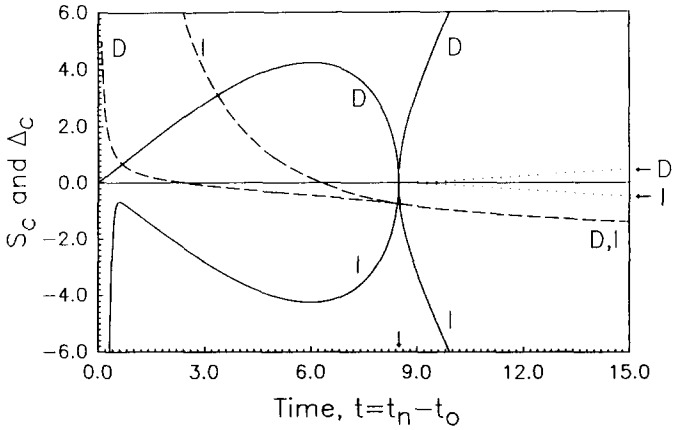

FIG. 9. The evolution of S_C (dashed lines for real part, light dotted lines for imaginary) and Δ_C (solid lines for both real and imaginary parts) for Paths D and I as $x_0 = 3$ and $x_n = 4$ are kept fixed, and t is varied. For $t < t_F$, Δ_C is purely real, and for $t > t_F$, it is purely imaginary. The arrow indicates $t_F = 8.485$.

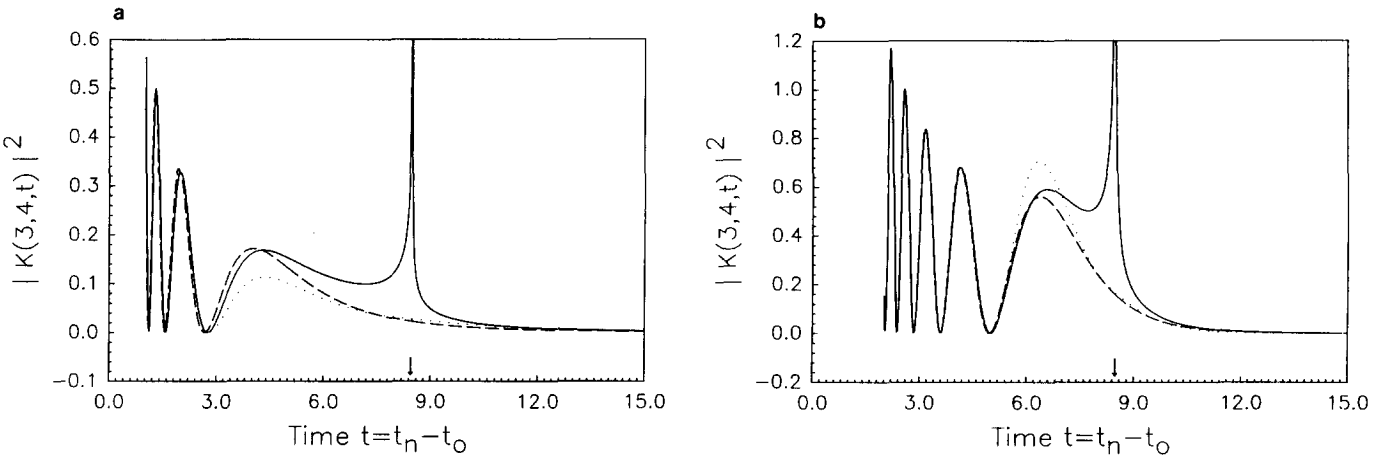

FIG. 10. The exact (dashed line), far-from-caustic WKB (solid line), and near-caustic WKB (dotted line) propagators, for propagating from $x_0 = 3$ to $x_n = 4$ in real times $0 < t < 15$, for (a) $\hbar = 1$ and (b) $\hbar = 0.258$. The arrow indicates $t_F = 8.485$.

Path I has action with $\mathrm{Im}(S_C) < 0$ and leads to an exponentially growing solution as $t \to \infty$. It is not included in $\sum_C$ in (14).

In Fig. 10 we compare the exact, far-from-caustic, and near-caustic WKB propagators for $\hbar = 1$ and 0.258, i.e., $\nu = \frac{3}{2}$ and $\frac{11}{2}$, for $x_0 = 3$, $x_n = 4$, and real times $0 < t < 15$. The WKB propagators are calculated using the paths obtained from the relaxation method. The agreement between the exact and far-from-caustic WKB propagators is remarkably good for times away from the caustic time $t_F = 8.485$, even for the very nonclassical value of $\hbar = 1$. (In our units $\hbar = 1$ is very nonclassical.) The near-caustic WKB propagator is also in good agreement with the exact value at $t = t_F$, but is poor over much of the caustic region for $\hbar = 1$; the agreement improves for $\hbar = 0.258$. For still smaller $\hbar$, this agreement improves further, and both the far-from-caustic and near-caustic WKB propagators match at the limits of the caustic region with increasing accuracy.

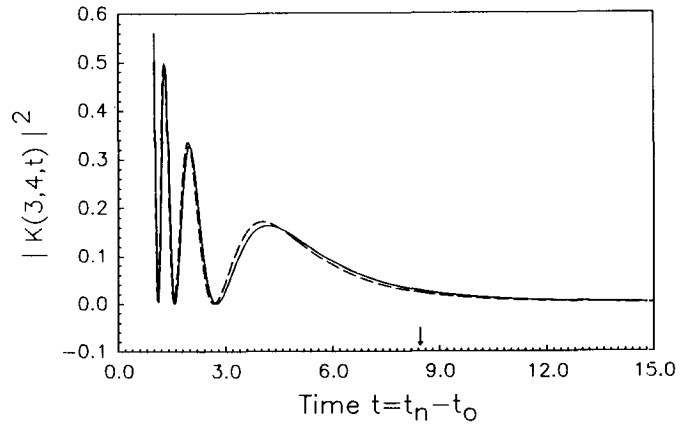

FIG. 11. The exact (dashed line) and uniform WKB (solid line) propagators, for propagating from $x_0 = 3$ to $x_n = 4$ in real times $0 < t < 15$ for $\hbar = 1$. The arrow indicates $t_F = 8.485$.

In cases where neither the near-caustic nor far-from-caustic form is accurate (e.g., the region $4 < t < 5$ for $\hbar = 1$; see Fig. 10a), the uniform approximation (see discussion below) gives a satisfactory result. In Fig. 11, the exact result and uniform approximation are compared for $\hbar = 1$. The agreement is seen to be quite satisfactory for all t. For smaller $\hbar$, the agreement is even better. Outside the caustic region, both the far-from-caustic and uniform approximation give about the same agreement with the exact result; but, near the caustic, the near-caustic form gives a substantially better result than the uniform approximation on the classically allowed side, is equal to the uniform result at the caustic, and is slightly worse than the uniform result on the classically unallowed side. Hence the near-caustic form is useful if greater accuracy is desired on the classically allowed side of the caustic; the price paid is the greater effort required in calculating the quantities which go into its form.

The uniform asymptotic approximation [2] for $K(x_0, x_n, t)$ is given by (14), but with a correction factor A_C inserted in the summand. For the generic case of two paths connecting each pair of end points and which coalesce at the caustic, A_C is given by [18, 19] $A_C = Ai^{(\pm)}(-q)$, where $(-)$ corresponds to $C = D$ (direct path), $(+)$ corresponds to $C = I$ (indirect path), and

$$Ai^{(\pm)}(-q) = \pi^{1/2}[q^{1/4}Ai(-q) \pm iq^{-1/4}Ai'(-q)] \times \exp\left(\mp i\left(\frac{2}{3}q^{3/2} - \frac{\pi}{4}\right)\right), \tag{33}$$

where $Ai'(x) = (d/dx)\,Ai(x)$, and q is defined by

$$\tfrac{4}{3}q^{3/2} = (S_I - S_D)/\hbar. \tag{34}$$

Note that $S_I - S_D = \tilde{S}_I - \tilde{S}_D$, since (see the argument of the exponential of Eq. (14)) S_I differs from $\tilde{S}_I$ by the same

amount as S_D differs from $\tilde{S}_D$. The factor A_C behaves as $A_C \to 1$ far from the caustic on the classically allowed side, and $A_C \to 0$ with finite product $A_C \Delta_C^{-1/2}$ near the caustic. On the classically unallowed side, $Ai^{(+)}$ suppresses the exponentially growing term, discarded in $\sum_C$ in (14), as discussed earlier; the growing term must be retained when the correction factor A_C is inserted. It is important to choose the phase of q correctly in (34). On the classically allowed side, q is to be taken as positive real, and on the unallowed side it is to be taken as negative real. The principal root in $q^{1/4}$ is to be taken in (33) in all cases.

ACKNOWLEDGMENTS

We gratefully acknowledge the Natural Sciences and Engineering Research Council of Canada for financial support of this work, and we thank a referee for bringing Ref. [11] to our attention.

REFERENCES

1. R. P. Feynman and A. R. Hibbs, *Quantum Mechanics and Path Integrals* (McGraw-Hill, New York, 1965).
2. L. S. Schulman, *Techniques and Applications of Path Integration* (Wiley, New York, 1981).
3. F. W. Wiegel, *Introduction to Path-Integral methods in Physics and Polymer Science* (World Scientific, Singapore, 1986).
4. The literature is extensive. For a review see Ref. [5]. Representative recent work is J. Schnitker and P. J. Rossky, *J. Phys. Chem.* **93**, 6965 (1989); M. Marchi, M. Sprik, and M. L. Klein, *J. Phys. Chem.* **94**, 431 (1990).
5. B. J. Berne and D. Thirumalai, *Ann. Rev. Phys. Chem.* **37**, 401 (1986).
6. U. S. Filinov, *Nucl. Phys. B* **271**, 717 (1986).
7. N. Makri and W. H. Miller, *Chem. Phys. Lett.* **139**, 10 (1987) and *J. Chem. Phys.* **89**, 2170 (1988).
8. J. D. Doll, T. L. Beck, and D. L. Freeman, *J. Chem. Phys.* **89**, 5753 (1988); T. L. Beck, J. D. Doll, and D. L. Freeman, *J. Chem. Phys.* **90**, 3181 (1989); J. D. Doll and D. L. Freeman, *Adv. Chem. Phys.* **73**, 289 (1989).
9. M. C. Gutzwiller, *J. Math. Phys.* **8**, 1979 (1967); P. Pechukas, *Phys. Rev.* **181**, 186 (1969); W. H. Miller, *J. Chem. Phys.* **53**, 1949, 3578 (1970); *Adv. Chem. Phys.* **25**, 69 (1974); J. N. L. Connor and R. A. Marcus, *J. Chem. Phys.* **55**, 5636 (1971); M. V. Berry and K. E. Mount, *Rep. Prog. Phys.* **35**, 315 (1972); J. N. L. Connor, *Mol. Phys.* **25**, 181 (1973); **26**, 1217 (1973); M. S. Child, *Mol. Phys.* **27**, 657 (1974); C. DeWitt-Morette, *Ann. Phys. (N.Y.)* **97**, 367 (1976); S. Levit and U. Smilansky, *Ann. Phys. (N.Y.)* **103**, 198 (1977); **108**, 165 (1977); S. Coleman, in *The Whys of Nuclear Physics*, edited by A. Zichichi (Plenum, New York, 1979); G. Dangelmayr and W. Veit, *Ann. Phys. (N.Y.)* **118**, 108 (1979); Y. Weissman, *J. Chem. Phys.* **76**, 4067 (1982); A. O. Caldeira and A. J. Leggett, *Ann. Phys. (N.Y.)* **149**, 374 (1983); C. DeWitt-Morette, B. Helson, and T. R. Zhang, *Phys. Rev. D* **28**, 2526 (1983); J. R. Klauder, *Ann. Phys. (N.Y.)* **180**, 108 (1987); N. Makri and W. H. Miller, *Chem. Phys. Lett.* **151**, 1 (1988); J. M. Leimaas and K. Olaussen, *Ann. Phys. (N.Y.)* **189**, 243 (1989); A. Ranfagni and D. Mugnai, *Nuovo Cimento D* **11**, 53 (1989); Z. H. Huang, T. E. Feuchtwang, P. H. Cutler, and E. Kazes, *Phys. Rev. A* **41**, 32 (1990).
10. S. Adachi, *Ann. Phys. (N.Y.)* **195**, 45 (1989).
11. J. D. Doll, T. L. Beck, and D. L. Freeman, *Int. J. Quant. Chem.; Quant. Chem. Symp.* **23**, 73 (1989). See also Beck *et al.*, (1989), Ref. [8] above.
12. Although both x and t dependence is arbitrary in V, we implicitly assume that V is a smooth funcion of x and t at sufficiently small time and length scales, so that V can be discretized in some meaningful way for the numerical method we present. In some of our examples, V is in fact time-independent.
13. S. E. Koonin, *Computational Physics* (Addison-Wesley, Reading, MA, 1986), p. 142.
14. A. Messiah, *Quantum Mechanics, Vol. 1* (North Holland, Amsterdam, 1961), p. 311.
15. The problems due to the Stokes lines and caustics are similar to those in WKB wave-functions at turning points. A successful means of dealing with this is by considering the wavefunctions in the complex x plane; see A. G. Basile, C. G. Gray, B. G. Nickel, and J. D. Poll, *Mol. Phys.* **66**, 961 (1989). An alternative approach, the uniform approximation, is considered here in Section 4.
16. W. H. Press, B. P. Flannery, S. A. Teukolsky, and W. T. Vetterling, *Numerical Recipes* (Cambridge Univ. Press, New York, 1986), p. 40. A generalization to complex tridiagonal matrices is required for the application described in this paper.
17. Ref. [16, pp. 360–363].
18. L. I. Lolle, J. D. Poll, and C. G. Gray, to be published.
19. S. Levit and U. Smilansky, *A Semiclassical Uniform Approximation for Path Integrals*, unpublished report (1976); see also Connor and Marcus (1971), and Connor (1973), Ref. [9] above.